SCOOP and STACK inversion case studies

Satinder Chopra[+], Ritesh Kumar Sharma[+], and James Keay[†]*

[+] TGS, Calgary; [†]TGS, Houston

Summary

The Mississippian section, in particular the Meramec and the Devonian Woodford continue to be the preferred investment targets in the SCOOP/STACK trend in Oklahoma We showcase here the seismic characterization of these formations using multicomponent seismic data in the STACK area and the conventional vertical component seismic data in the SCOOP area, using deterministic prestack impedance inversion. The joint impedance inversion carried out over seismic data from the STACK area was used to derive rock-physics parameters (Young's modulus and Poisson's ratio), which showed the sweet spots that are distinct spatially, rather than bleeding off at the edges. The added advantage of joint inversion was that the density attribute could also be derived therefrom, which was not possible for the data from the STACK area. In addition to density, the results from prestack joint impedance inversion have been found to be superior to the simultaneous inversion. The equivalent attributes (besides density) derived for the SCOOP area also show promise.

Introduction

The Oklahoma SCOOP play extend about 200 miles along the east flank of the Anadarko Basin, and along with the STACK play, have become one of the most active unconventional plays in the US. The trend has gathered attention due to its potential for oil and liquids-rich gas yields, record-setting IP from wells, superior economics and proximity to pipelines and infrastructure. Consequently, oil companies are making huge investments in these plays.

SCOOP is an acronym for South Central Oklahoma Oil Province, and is spread over Carter, Garvin, Grady, McClain, Stephens, Jefferson, Love, Caddo, and Murray counties in Oklahoma. STACK stands for Sooner Trend (in) Anadarko (basin) Canadian and Kingfisher (counties). Most of the play is located across Canadian and Kingfisher counties, together with Blaine, Dewey (far west), Major, and Garfield (far north) counties. The SCOOP refers to geographic location while the STACK, also geographic, alludes to the considerable multi-zone potential in that area.

Though the main target formations in the STACK are the Woodford and Meramec, operators have also been exploiting the Permian Oswego, Mississippian Chester and Osage, as well as the Siluro-Devonian Hunton Formation, (Figure 1). The Meramec formation has overpressured oil with low water content that creates high initial production (IP) rates. Due to lower water disposal requirements, the wells prove to be economical. The Woodford and Hunton are also drilled in the STACK play, but in addition, other formations exploited are the Caney, Hoxbar, and Springer Shale. Industry continues to identify and evaluate areas within these formations for favorable parameters that translate into lower completion costs and improved initial recoveries

In Figure 1 we show a segment of a seismic section from the STACK area which has a sonic log curve overlaid on it at the location of a well, as well as a lithostrip which shows the formations of interest in this area. The Woodford shale is the primary source rock in this area, and has served as a source rock to many other formations above and below it. The focus of the present study is to test characterization of the Woodford and Meramec formations in terms of identification of sweet spots that may represent more favorable drilling targets. Among other attributes generated for this exercise, prestack impedance inversion was carried out on two different seismic volumes, one from the STACK, and the other from the SCOOP area.

Seismic data acquisition and processing

Two 3D seismic data volumes were acquired, one within the STACK area, and the other over the SCOOP area. The acquisition of a 756 mi^2 (1958 km^2) 3C3D seismic data was completed in October 2014 over Blaine, Canadian, and Kingfisher counties of Oklahoma. The acquisition parameters included 220 ft (67.1 m) for source and receiver intervals, 880 ft (268 m) for source-line spacing, 1320 ft (402 m) for receiver-line spacing, maximum offset as 25466 ft (7762 m), 2 ms sample interval, fold 190, 5 s record length, which yielded a bin size of 110 x 110 ft (33.5 x 33.5 m). Three vibrator sweeps of 12 s were used as the seismic source. The processing of this volume was completed with Q phase-only correction, radon demultiple, prestack time migration gathers and stacked volume with 5D interpolation made available for impedance inversion exercise. As this was 3C data, we received the access to both the prestack as well as stacked PP and PS seismic data. The other seismic dataset in the SCOOP area was acquired in October 2015 over Grady and McClain counties in Oklahoma. The acquisition parameters included 220 ft (67.1 m) for source and receiver intervals, 880 ft (268 m) for source line spacing, 1100 ft (335.3 m) for receiver line spacing, maximum offset as 22981 ft (7004.6 m), 2 ms sample interval, fold 208, 5 s record length, which yielded a bin size of 110 x 110 ft (33.5 x 33.5 m). Three vibrators were used as the seismic source with a nonlinear sweep length of 32 s. The processing of this volume was completed with Q correction, 5D interpolation and anisotropic prestack time migration.

Well-log correlation

Figure 2 shows the well-log correlation where the P-impedance, S-impedance and density curves for well W-3, as well as PS synthetic seismogram are shown correlated with PP and PS seismic data in PS two-way time. A zero-phase wavelet (shown on the top in Figure 2) was estimated from the seismic data using a statistical process. The synthetic PS traces are in blue, the field PS traces in red, and we notice a good correlation (84%) overall.

Preconditioning of seismic data

The preconditioning of seismic data (PP and PS) is carried out carefully to make sure that amplitudes are preserved such that their variation with offset or angle could be used in a meaningful way. The major processes used in the conditioning are supergathering (3x3), band-pass filtering, random noise attenuation, and trim statics, with difference plots taken at each step to ensure that no useful signal was distorted or attenuated (Hunt et al., 2015; Chopra and Sharma, 2016). The PP gathers are picked up first for running prestack simultaneous impedance inversion, followed by PP and PS gathers for running prestack joint inversion.

Low-frequency trend determination for impedance inversion

While carrying out impedance inversion, the addition of a low-frequency trend is necessary for obtaining absolute values of impedance. The usual practice is to low-pass filter (< 10 Hz) the available impedance well-log curves and use one or more of the derived curves for generation of the low-frequency trend volume using extrapolation or interpolation and guided by horizon boundaries. When more than one well is used for the generation of the low-frequency trend, usually an inverse-distance weighted scheme or a process called kriging is utilized. Such techniques need to be used with care as they can produce artifacts. We make use of a relatively new approach for low-frequency trend generation that makes use of both well log data as well as seismic data to establish a relationship between seismic attributes and the available well log curves. Using the low-frequency model generated with a single well as one of the inputs, and some other seismic data volumes, a multi-regression approach (as described in Ray and Chopra, 2016) is used, wherein a target log is modeled as a linear combination of several input attributes at each sample point which in this case happen to be the relative acoustic impedance, some instantaneous attributes and different versions of the filtered seismic data. The low-frequency impedance models for simultaneous and joint inversions are generated using the above approach.

Simultaneous inversion

In simultaneous inversion, multiple partial-offset or angle substacks are inverted simultaneously. For each angle stack, a unique wavelet is estimated. Subsurface low-frequency models for P-impedance, and S-impedance constrained with appropriate horizons in the broad zone of interest, are constructed using the approach explained above. The models, wavelets and partial stacks are used as input in the inversion, and the output is P-impedance and S-impedance. An arbitrary line from the inverted P-impedance volume and passing through 4 wells on the 3D seismic volume is shown in Figure 3. We notice the lateral variation of P-impedance across the line, and its correlation with the overlaid P-impedance curves seems to be acceptable. Because the useable angle range for simultaneous inversion is 39º, a useable density attribute could not be extracted.

Joint inversion

Inversion of P-wave data together with S-wave data is referred to as *joint inversion*. Joint inversion makes use of the amplitudes and travel times of the P-wave and S-wave data for estimating P-impedance, S-impedance and density attributes that provide a more robust means of interpretation. After processing of multicomponent seismic data, the outputs are PP wave data processed in PP two-way time and PS wave data processed in PS time scale. For carrying out any consistent analysis, the first step is to carry out an accurate PP and PS time correspondence, which is accomplished by tying with PP and PS synthetic seismograms respectively, generated over the same range of frequency bandwidth as the input reflection data. This process is referred to as *registration*. It is usually carried out by matching the corresponding correlative events on the PP and PS data volumes, and then mapping or shrinking the PS time scale to the PP time scale. Once the well-to-seismic correlation for both PP and PS data is done satisfactorily (shown in Figure 2), the depth-time curves for both get determined. The V_P/V_S ratio determined this way is valid at the location of the well only. Using this information, the PP data with its horizons are stretched to PS time, and displayed alongside PS data (in PS time). This helps identify the corresponding horizons on the PS data, and the trackable horizons are then picked. The horizons picked on PP and PS data will match at the location of the wells, but laterally will exhibit travel-time differences. Such differences are determined for the different intervals bounded by horizons and V_P/V_S ratios determined for those intervals as per the equation below.

$$\frac{V_\mathrm{P}}{V_\mathrm{S}} = 2\left(\frac{PS\ isochron}{PP\ isochron}\right) - 1$$

In Figure 3 we show the horizons picked on PP and PS seismic data correlated with V_P/V_S log curves from W-3. The V_P/V_S velocity field is seen in the background after horizon matching. On the PS panel the horizons picked on both datasets are matched and the differences in color are seen after the adjustment of V_P/V_S values. The PS data are shown in PP two-way time. The generated V_P/V_S wavefield was confirmed at some blind wells and so it was taken to be accurate.

For prestack joint inversion, three angle-limited stacks for PP and five stacks for PS data are first generated. A common issue with the multicomponent seismic data is that the frequency content of PS data is lower than the frequency content of the PP seismic data, which is not desirable when we carry out joint impedance inversion. We have tried to address this issue by frequency balancing the near-, mid- and far- stack for both PP and PS in an AVO friendly way. The modeled reflectivities at these angles are then generated, compared with the real data and the error between them is then minimized in a least squares sense. The output from the joint inversion is P-impedance, S-impedance and density data. An arbitrary line equivalent to the one shown in Figure 4a, from the inverted P-impedance volume (joint inversion) is shown in Figure 4b. Notice the joint inversion looks much better than the simultaneous impedance inversion. An equivalent density section is also shown in Figure 4c.

Impedance inversion analysis

We begin by crossplotting the P-impedance and V_P/V_S from well-log data for W-3 between the Meramec to Woodford interval as shown in Figure 5. The cluster points on the crossplot have been color-coded with density, and we notice that data points with lower values of density also exhibit lower P-impedance and lower V_P/V_S as expected.

We generated equivalent crossplots for P-impedance and V_P/V_S for the inverted volumes obtained with simultaneous and joint impedance inversions, which are shown in Figures 6a and b.

We notice, that the crossplot from simultaneous inversion has a larger spread than the one we got from the log data. This is perhaps due to the larger number of inverted data traces brought into the crossplot, but the equivalent crossplot from joint inversion shows a tighter spread, and has a shape similar to the one obtained from well-data.

We take this analysis forward in that we generate attributes such as Poisson's ratio, Young's modulus (E-rho, Sharma and Chopra, 2015), and some others, in order to determine brittleness of the Woodford formation. In Figure 7 we show a comparison of horizon slices averaged in a 20 ms above the Woodford marker from the Poisson's ratio and E-rho volumes derived from simultaneous inversion and joint inversion. We notice clearly on these displays that the pockets showing lower values of these attributes are seen as more compact.

For the other 3D seismic volume from the SCOOP area, as only the vertical component data was available, we performed simultaneous inversion similar to the one from the STACK area after frequency balancing of near-, mid- and far- stacks. We include a horizon slice from the inverted V_P/V_S volume overlaid with energy-ratio coherence in Figure 8. Details of the workflow and results will be presented in the formal presentation.

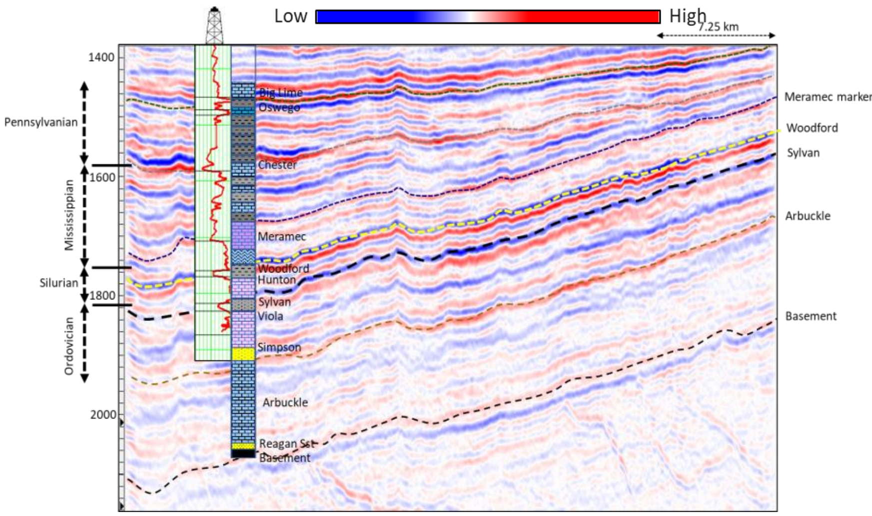

Figure 1: A segment of an inline from the northern part of the 3D seismic volume and passing through a well. The overlaid sonic curve and lithostrip illustrate the lithology of the formations of interest and their relative thicknesses. *(Data courtesy: TGS, Houston)*

Figure 2: Well log correlation with PP and PS seismic data for well W-3. The synthetic PS traces are in blue and are being compared with the PS field traces in red. All data are displayed in PS two-way time. A good correlation (84%) is seen between the synthetic and real traces. *(Data courtesy: TGS, Houston)*

Conclusions

We performed seismic reservoir characterization of the Woodford and Meramec formations in the STACK and SCOOP areas of Oklahoma. The seismic attributes derived from joint impedance inversion (as multicomponent data was available) in the STACK area have shown better quality than equivalent attributes using simultaneous impedance inversion. Another advantage is that we were able to derive the density attribute from joint inversion, whereas the PP prestack data did not have the angle range required for determination of density. In the SCOOP area, only the vertical component 3D seismic data was recorded, and thus we could only carry out simultaneous inversion. Nevertheless, the inversion attributes and the subsequent rock physics parameters were useful.

Acknowledgements

We wish to thank TGS, Calgary for encouraging this work and permission to present.

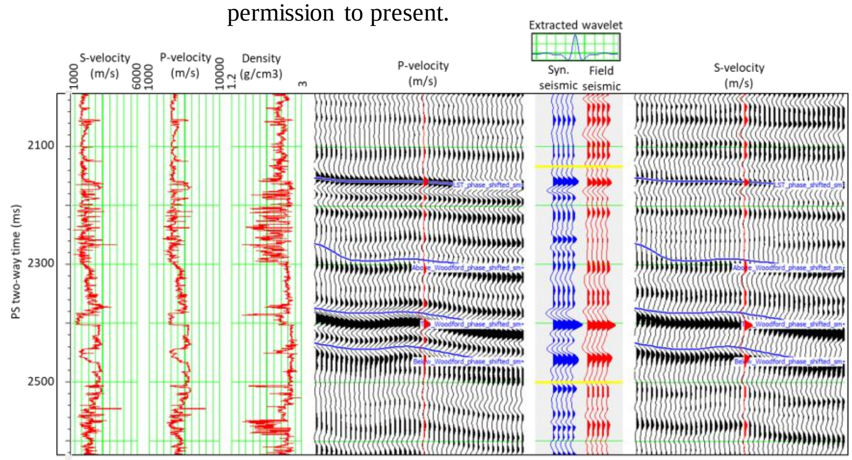

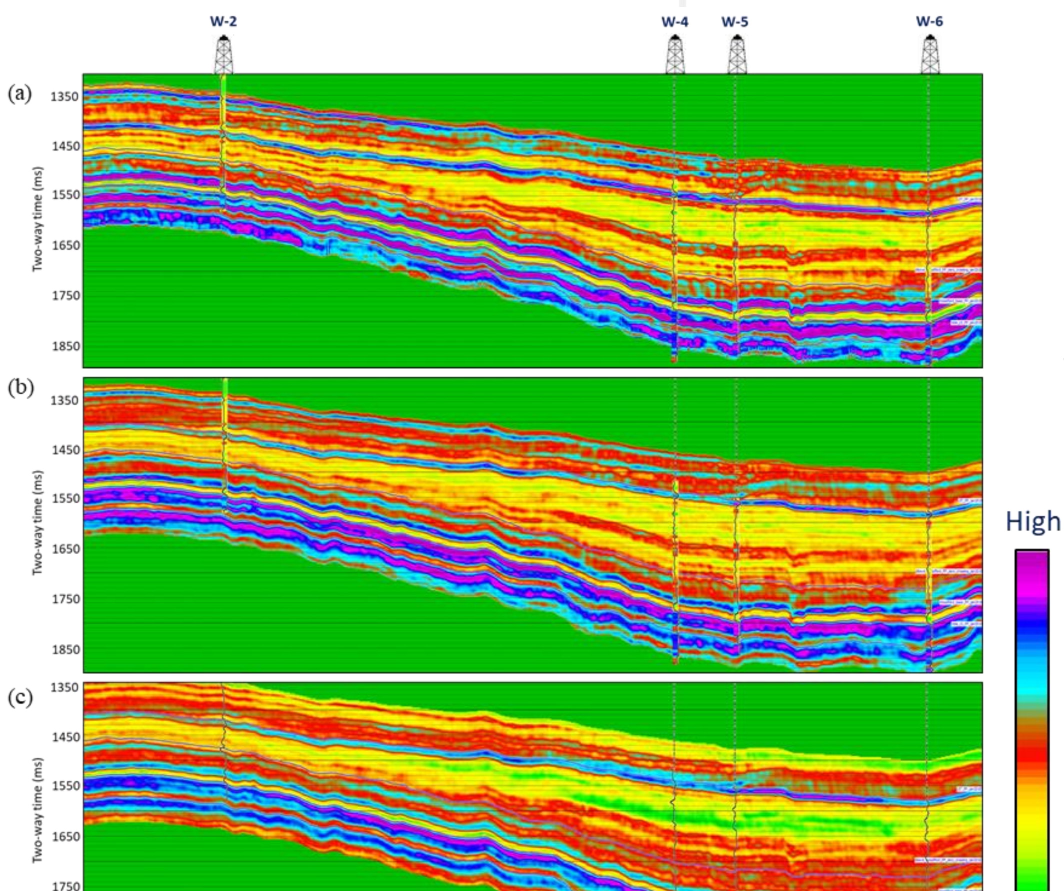

Figure 4: An arbitrary line from the P-impedance volume generated using (a) prestack simultaneous impedance inversion, (b) prestack joint impedance inversion, passing through four different wells. The overlaid curves are the P-impedance curves at the well locations. The location of the wells on the 3D seismic volume are shown in Figure 7. In (c) we show an equivalent density section generated using prestack joint inversion, but could not be generated using simultaneous inversion due to inadequate angle range. *(Data courtesy: TGS, Houston)*

10.1190/segam2018-2997345.1

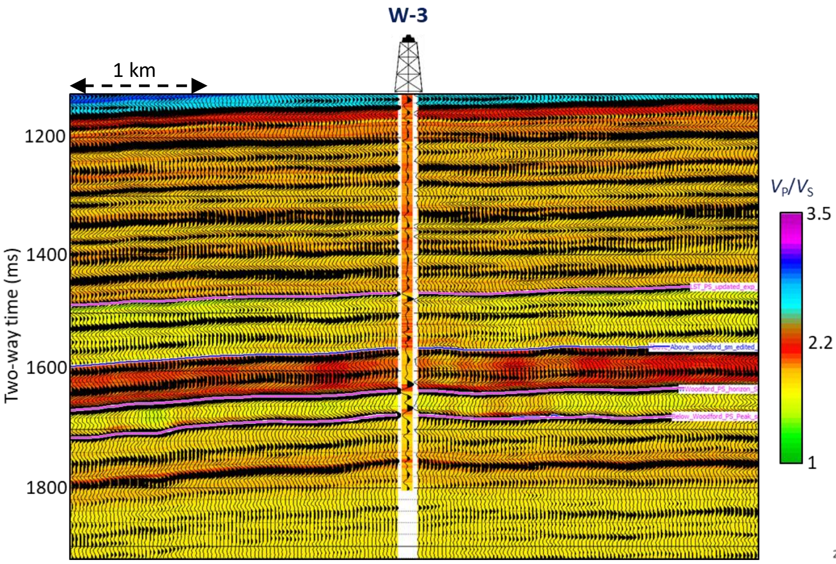

Figure 3: Horizons picked on PP and PS seismic data are correlated with the V_P/V_S log curves from well W-3. The V_P/V_S velocity field is seen in the background after horizon matching. On the PS data panel the horizons picked on both datasets are shown overlaid and no travel-time differences are seen. The differences in colour are seen after adjustment of V_P/V_S values on horizon matching. Both datasets are in PP two-way time. *(Data courtesy: TGS, Houston)*

.

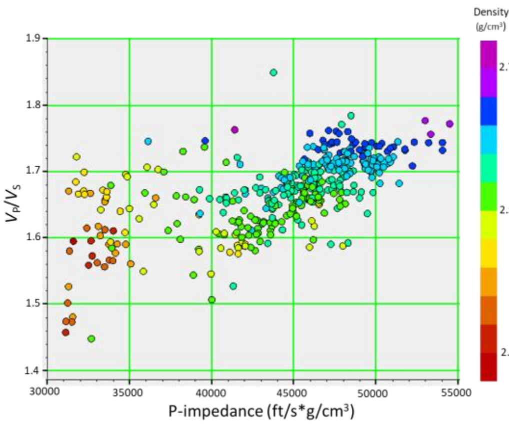

Figure 5: Crossplot between P-impedance and V_P/V_S, colour coded with density using well-log data from Meramec to base of Woodford formation. *(Data courtesy: TGS, Houston)*

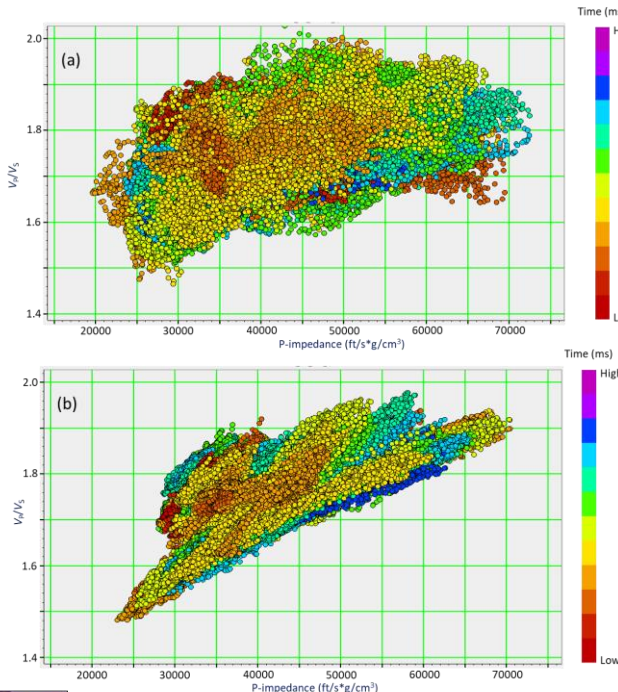

Figure 6: Crossplot between inverted P-impedance and V_P/V_S, generated using (a) simultaneous inversion, and (b) prestack joint impedance inversion. The cluster points are colour-coded with time along the arbitrary line over an interval from Meramec to base of Woodford. *(Data courtesy: TGS, Houston)*

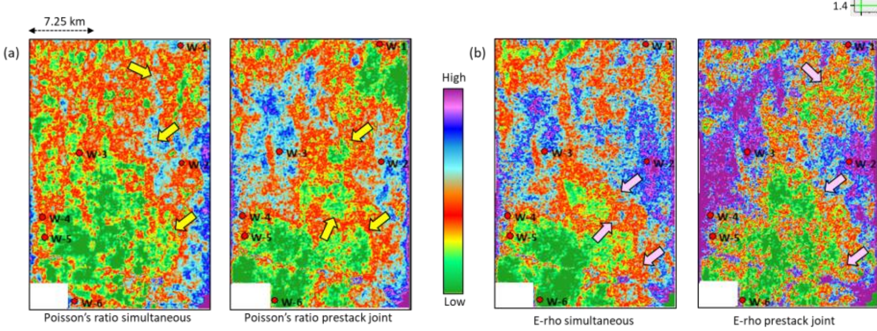

Figure7: Horizon slices from (a) inverted Poisson's ratio using simultaneous and prestack joint inversion, and (b) inverted E-rho using simultaneous and prestack joint inversion, over a 20 ms window above the Woodford base horizon. The distribution of the low values of Poisson's ratio and E-rho from joint inversion displays seems to be more realistic and distinct that the equivalent displays from simultaneous inversion. *(Data courtesy: TGS, Houston)*

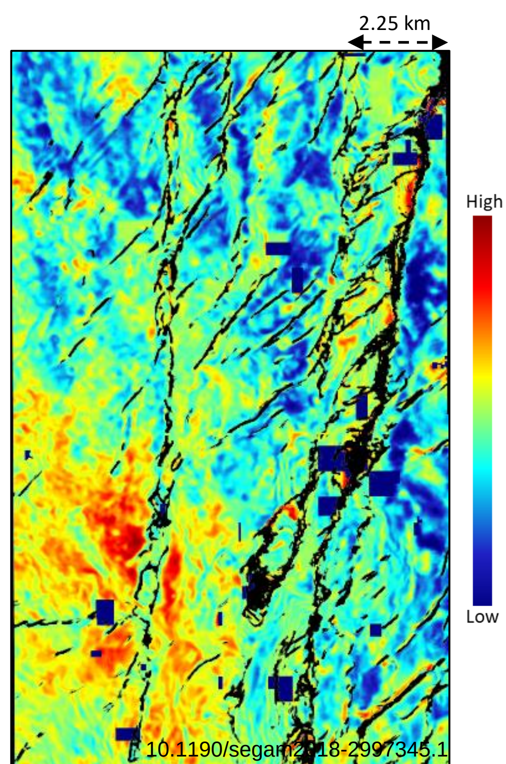

Figure 8: Horizon slice from inverted V_P/V_S ratio volume generated using simultaneous inversion, close to the Woodford base horizon for the seismic data volume from the SCOOP area. The low values of V_P/V_S ratio are seen to be in pockets that are strewn with faults and fractures. This observation needs to be confirmed with well data, an exercise that will be carried out shortly. *(Data courtesy: TGS, Houston)*

10.1190/segam2018-2997345.1

REFERENCES

Chopra, S., and R. K. Sharma, 2016, Preconditioning of seismic data prior to impedance inversion: AAPG Explorer, **37**, 30–33.
Hunt, L., P. Cary, D. Tican, M. Perz, R. K. Sharma, N. Nagarajappa, X. Li, S. Chopra, 2015, VOQC. Value oriented quality control in seismic processing: CSEG Recorder, **40**, 42–51.
Ray, A. K., and S. Chopra, 2016, Building more robust low-frequency models for seismic impedance inversion: First Break, **34**, 29–34, https://doi.org/10.3997/1365-2397.2016005.
Sharma, R. K., and S. Chopra, 2015, Determination of lithology and brittleness of rocks with a new attribute: The Leading Edge, **34**, 936–941, https://doi.org/10.1190/tle34050554.1.

10.1190/segam2018-2997345.1